Supplement of Atmos. Chem. Phys., 14, 5807–5824, 2014
http://www.atmos-chem-phys.net/acp-14-5807-2014/
doi:10.5194/acp-14-5807-2014-supplement

Atmospheric Chemistry and Physics Open Access

Supplement of

Estimating Asian terrestrial carbon fluxes from CONTRAIL aircraft and surface CO_2 observations for the period 2006–2010

H. F. Zhang et al.

Correspondence to:

Table S1 Summary of the global surface CO_2 observation data assimilated between January 1, 2006 and December 31, 2010. The frequency of continuous data is one data point per day (when available), while discrete surface data point is generally once per week. MDM (model-data-mismatch) is a value assigned to a given site that is meant to quantify our expected ability to simulate observations and used to calculate the innovation X^2 (Inn. X^2) statistic. N denotes that the number is available in the CTDAS. Flagged observations mean the model-minus-observation difference if it exceeds 3 times of the model-data-mismatch and therefore is excluded from assimilation. The bias is the average from posterior residuals (assimilated values–measured values), while the modeled bias is the average from prior residuals (modeled values–measured values). Laboratory abbreviations refer to the description of the GLOBALVIEW product (Masarie and Tans, 1995).

Site	Name	Lat, Lon, Elev.	Lab	N(flagged)	MDM	Inn. X^2	Bias(modeled)
'abp_01d0'	Arembepe, Bahia, Brazil	12.77°S,38.17°W,1m	ESRL	102(0)	3	0.3	-1.18(-1.51)
'abp_26d0'	Arembepe, Bahia, Brazil	12.77°S,38.17°W,1m	IPEN	101(0)	3	0.38	-1.33(-1.67)
'alt_01d0'	Alert, Nunavut, Canada	82.45°N,62.51°W,200m	ESRL	246(0)	1.5	0.43	0.01(0.12)
'alt_06c0'	Alert, Nunavut, Canada	82.45°N,62.51°W,200m	EC	1590(0)	2.5	0.21	0.18(0.27)
'amt_01c3'	Argyle, Maine, United States	45.03°N,68.68°W,50m	ESRL	1571(59)	3	0.98	0.8(0.83)
'amt_01d0'	Argyle, Maine, United States	45.03°N,68.68°W,50m	ESRL	126(0)	1000	0	-0.11(0.14)
'amt_01p0'	Argyle, Maine, United States	45.03°N,68.68°W,50m	ESRL	307(0)	1000	0	0.69(0.52)
asc_01d1'	Ascension Island, United Kingdom	7.92°S,14.42°W,54m	ESRL	413(2)	0.75	0.91	-0.09(-0.14)
'ask_01d0'	Assekrem, Algeria	23.18°N,5.42°E,2728m	ESRL	221(0)	1.5	0.34	-0.11(-0.12)
'azr_01d0'	Terceira Island, Azores, Portugal	38.77°N,27.38°W,40m	ESRL	136(3)	1.5	0.96	0.36(0.39)
'bal_01d0'	Baltic Sea, Poland	55.35°N,17.22°E,3m	ESRL	473(0)	7.5	0.38	0.11(0.23)
'bao_01c3'	Boulder Atmospheric Observatory, Colorado, United States	40.05°N,105.00°W,1584m	ESRL	1482(42)	3	1.02	-0.46(0.11)
'bao_01p0'	Boulder Atmospheric Observatory, Colorado, United States	40.05°N,105.00°W,1584m	ESRL	760(0)	1000	0	-1.78(-1.47)
'bhd_01d0'	Baring Head Station, New Zealand	41.41°S,174.87°E,85m	ESRL	82(0)	1.5	0.3	0.09(0.09)
'bkt_01d0'	Bukit Kototabang, Indonesia	N,100.32°E,864m	ESRL	172(0)	7.5	0.73	5.53(5.51)
'bme_01d0'	St. Davids Head, Bermuda,	32.37°N,64.65°W,30m	ESRL	47(0)	1.5	0.75	0.17(0.21)

	United Kingdom						
'bmw_01d0'	Tudor Hill, Bermuda, United Kingdom	32.27°N,64.88°W,30m	ESRL	143(3)	1.5	0.69	0.19(0.21)
'brw_01c0'	Barrow, Alaska, United States	71.32°N,156.61°W,11m	ESRL	1319(1)	2.5	0.28	0.35(0.55)
'brw_01d0'	Barrow, Alaska, United States	71.32°N,156.61°W,11m	ESRL	227(2)	1.5	0.6	0.12(0.35)
'bsc_01d0'	Black Sea, Constanta, Romania	44.17°N,28.68°E,3m	ESRL	149(7)	7.5	1.33	-4.08(-3.85)
'cba_01d0'	Cold Bay, Alaska, United States	55.21°N,162.72°W,21m	ESRL	290(17)	1.5	1.28	-0.49(-0.42)
cdl_06c30'	Candle Lake, Saskatchewan, Canada	53.99°N,105.12°W,600m	EC	825(9)	3	0.7	0.79(1.5)
cfa_02d0'	Cape Ferguson, Queensland, Australia	19.28°S,147.06°E,2m	CSIRO	96(0)	2.5	0.43	-0.95(-1.19)
'cgo_01d0'	Cape Grim, Tasmania, Australia	40.68°S,144.69°E,94m	ESRL	156(0)	0.75	0.27	-0.06(-0.09)
'cgo_02d0'	Cape Grim, Tasmania, Australia	40.68°S,144.69°E,94m	CSIRO	154(1)	0.75	0.25	-0.12(-0.14)
'chr_01d0'	Christmas Island, Republic of Kiribati	1.70°N,157.17°W,3m	ESRL	192(0)	0.75	1.11	-0.59(-0.65)
'cri_02d0'	Cape Rama,India	15.08°N,73.83°E,60m	CSIRO	33(1)	3	1.4	-1.97(-2.11)
'crz_01d0'	Crozet Island, France	46.45°S,51.85°E,120m	ESRL	217(0)	0.75	0.2	-0.09(-0.14)
'cya_02d0'	Casey, Antarctica, Australia	66.28°S,110.52°E,51m	CSIRO	97(0)	0.75	0.32	-0.28(-0.32)
'egb_06c0'	Egbert, Ontario, Canada	44.23°N,79.78°W,251m	EC	1001(73)	3	1.28	0.88(1.33)
'eic_01d0'	Easter Island, Chile	27.15°S,109.45°W,50m	ESRL	153(0)	7.5	0.02	0.53(0.51)
'esp_06c0'	Estevan Point, British Columbia, Canada	49.38° N ,126.54°W,7m	EC	614(19)	3	0.63	-0.33(-0.25)
'etl_06c0'	East Trout Lake, Saskatchewan, Canada	54.35°N,104.98°W,492m	EC	1063(6)	3	0.51	0.22(0.75)
'fef_03c0'	Fraser, Colorado, United States	39.91°N,105.88°W,2745m	NCAR	2558(158)	3	0.85	-0.43(-0.42)
'gmi_01d0'	Mariana Islands, Guam	13.43°N,144.78°E,3m	ESRL	249(0)	1.5	0.29	-0.09(-0.11)
'gsn_61c0'	Gosan, Republic of Korea	33.15°N,126.12°E,72m	NIER	1274(109)	3	1.99	-1.01(-0.82)
'hba_01d0'	Halley Station, Antarctica, United Kingdom	75.61°S,26.21°W,30m	ESRL	205(0)	0.75	0.22	-0.21(-0.26)
'hdp_03c0'	Hidden Peak (Snowbird), Utah, United States	40.56°N,111.65°W,3351m	NCAR	2285(1)	3	0.27	-0.29(-0.28)
'hpb_01d0'	Hohenpeissenberg, Germany	47.80°N,11.01°E,985m	ESRL	208(0)	7.5	0	2.77(2.86)
'hun_01d0'	Hegyhatsal, Hungary	46.95°N,E,248m	ESRL	232(0)	7.5	0.39	0.35(0.5)
'ice_01d0'	Storhofdi, Vestmannaeyjar, Iceland	63.40°N,20.29°W,118m	ESRL	222(2)	1.5	0.7	-0.39(-0.35)
'izo_01d0'	Izana, Tenerife, Canary Islands, Spain	28.31°N,16.50° W,2372.9m	ESRL	207(0)	1.5	0.72	0.63(0.62)
'key_01d0'	Key Biscayne, Florida, United States	25.67°N,E,3m	ESRL	147(0)	2.5	0.23	-0.04(-0.02)
'kum_01d0'	Cape Kumukahi, Hawaii, United States	19.52°N,154.82°W,3m	ESRL	289(0)	1.5	0.44	-0.21(-0.21)
'kzd_01d0'	Sary Taukum, Kazakhstan	44.06°N,76.82°E,601m	ESRL	167(6)	2.5	1.16	-0.08(0.5)
'kzm_01d0'	Plateau Assy, Kazakhstan	43.25°N,77.88°E,2519m	ESRL	155(2)	2.5	0.96	0.5(0.63)
'lef_01c3'	Park Falls, Wisconsin, United	45.95°N,90.27°W,472m	ESRL	2267(55)	3	0.87	0.2(0.52)

	States						
'lef_01d0'	Park Falls, Wisconsin, United States	45.95°N,90.27°W,472m	ESRL	227(0)	1000	0	0.76(1.09)
'lef_01p0'	Park Falls, Wisconsin, United States	45.95°N,90.27°W,472m	ESRL	1341(0)	1000	0	0.11(0.41)
'llb_06c0'	Lac La Biche, Alberta, Canada	54.95°N,112.45°W,540m	EC	1206(43)	3	1	0.14(0.5)
'lln_01d0'	Lulin,Taiwan	23.47° N,120.87°E,2862m	ESRL	220(20)	7.5	0.99	2.62(2.65)
'lmp_01d0'	Lampedusa, Italy	35.52°N,12.62°E,45m	ESRL	197(0)	1.5	0.91	0.05(0.07)
'maa_02d0'	Mawson Station, Antarctica, Australia	67.62°S,E,32m	CSIRO	87(0)	0.75	0.34	-0.29(-0.32)
'mhd_01d0'	Mace Head, County Galway, Ireland	53.33°N,9.90°W,5m	ESRL	180(0)	2.5	0.18	0(0)
'mid_01d0'	Sand Island, Midway, United States	28.21°N,177.38°W,4m	ESRL	229(0)	1.5	0.74	0.22(0.22)
'mkn_01d0'	Mt. Kenya, Kenya	0.05°S,37.30°E,3897m	ESRL	74(0)	2.5	1.08	1.59(1.56)
'._01c0'	Mauna Loa, Hawaii, United States	19.54°N,155.58°W,3397m	ESRL	1420(4)	0.75	0.55	0.06(0.06)
'mlo_01d0'	Mauna Loa, Hawaii, United States	19.54°N,155.58°W,3397m	ESRL	251(0)	1.5	0.15	0.01(0.02)
'mnm_19c0'	Minamitorishima,Japan	24.29°N,153.98°E,8m	JMA	1624(0)	3	0.76	0.15(0.16)
'mqa_02d0'	Macquarie Island, Australia	54.48°S,158.97°E,12m	CSIRO	114(0)	0.75	0.3	-0.05(-0.07)
'nmb_01d0'	Gobabeb, Namibia	23.58°S,15.03°E,456m	ESRL	142(0)	2.5	0.19	-0.54(-0.58)
'nwr_01d0'	Niwot Ridge, Colorado, United States	40.05°N,105.58°W,3523m	ESRL	226(4)	1.5	0.62	0.21(0.18)
'nwr_01p0'	Niwot Ridge, Colorado, United States	40.05°N,105.58°W,3523m	ESRL	869(31)	1.5	1	0.44(0.43)
'obn_01d0'	Obninsk, Russia	55.11°N,36.60°E,183m	ESRL	68(5)	7.5	0.64	-1.51(-1.29)
'oxk_01d0'	Ochsenkopf, Germany	50.03°N,11.80°E,1022m	ESRL	139(10)	2.5	1.32	-0.18(-0.11)
'pal_01d0'	Pallas-Sammaltunturi, GAW Station, Finland	67.97°N,24.12°E,560m	ESRL	225(3)	2.5	0.74	0.06(0.32)
'poc_01d1'	Pacific Ocean, N/A	0.39°S,132.32°W,10m	ESRL	853(10)	0.75	0.79	-0.07(-0.1)
'psa_01d0'	Palmer Station, Antarctica, United States	64.92°S,64.00°W,10m	ESRL	247(0)	0.75	0.43	-0.27(-0.35)
'pta_01d0'	Point Arena, California, United States	38.95°N,123.74°W,17m	ESRL	200(0)	7.5	0.34	-2.19(-2.08)
'rpb_01d0'	Ragged Point, Barbados	13.17°N,59.43°W,45m	ESRL	227(0)	1.5	0.57	-0.15(-0.17)
'ryo_19c0'	Ryori,Japan	39.03°N,141.82°E,260m	JMA	1663(48)	3	0.9	0.46(0.69)
'sdz_01d0'	Shangdianzi, China	40.39°N,117.07°E,287m	CMA/ESRL	60(15)	3	1.18	0.15(0.18)
'sey_01d0'	Mahe Island, Seychelles	4.67°S,55.17°E,3m	ESRL	221(5)	0.75	0.77	-0.07(-0.08)
'sgp_01d0'	Southern Great Plains, Oklahoma, United States	36.80°N,97.50°W,314m	ESRL	225(13)	2.5	1.28	-0.51(-0.14)
'shm_01d0'	Shemya Island, Alaska, United States	52.72°N,174.10°E,40m	ESRL	149(0)	2.5	1.02	-0.11(-0.05)
'smo_01c0'	Tutuila, American Samoa	14.25°S,170.56°W,42m	ESRL	1598(0)	0.75	0.49	0.1(0.09)

'smo_01d0'	Tutuila, American Samoa	14.25°S,170.56°W,42m	ESRL	239(0)	1.5	0.16	-0.06(-0.09)
'snp_01c3'	Shenandoah National Park, United States	38.62°N,78.35°W,1008m	ESRL	1237(98)	3	1.5	-0.14(0.04)
'spl_03c0'	Storm Peak Laboratory (Desert Research Institute), United States	40.45°N,106.73°W,3210m	NCAR	1874(14)	3	0.62	-0.68(-0.69)
'spo_01d0'	South Pole, Antarctica, United States	89.98°S,24.80°W,2810m	ESRL	238(0)	1.5	0.04	-0.16(-0.2)
'stm_01d0'	Ocean Station M, Norway	66.00°N,2.00°E,0m	ESRL	343(3)	1.5	0.68	0.16(0.28)
'str_01p0'	Sutro Tower, San Francisco, California, United States	37.76°N,122.45°W,254m	ESRL	698(0)	1000	0	-0.27(-0.14)
'sum_01d0'	Summit, Greenland	72.58°N,38.48°W,3238m	ESRL	248(0)	1.5	0.47	0.16(0.21)
'syo_01d0'	Syowa Station, Antarctica, Japan	69.00°S,39.58°E,11m	ESRL	114(0)	0.75	0.22	-0.24(-0.28)
'tap_01d0'	Tae-ahn Peninsula, Republic of Korea	36.73°N,126.13°E,20m	ESRL	181(3)	7.5	0.6	1.82(2.13)
'tdf_01d0'	Tierra Del Fuego, Ushuaia, Argentina	54.87°S,68.48°W,20m	ESRL	117(0)	0.75	0.74	-0.36(-0.42)
'thd_01d0'	Trinidad Head, California, United States	41.05°N,124.15°W,107m	ESRL	232(21)	2.5	1.33	-1.49(-1.56)
'uta_01d0'	Wendover, Utah, United States	39.90°N,113.72°W,1320m	ESRL	220(11)	2.5	0.76	0.65(0.98)
'uum_01d0'	Ulaan Uul, Mongolia	44.45°N,111.10°E,914m	ESRL	231(5)	2.5	1.17	0.1(0.28)
'wbi_01c3'	West Branch, Iowa, United States	41.72°N,91.35°W,242m	ESRL	1801(141)	3	1.21	0.22(0.64)
'wbi_01p0'	West Branch, Iowa, United States	41.72°N,91.35°W,242m	ESRL	845(0)	1000	0	0.36(0.81)
'wgc_01c3'	Walnut Grove, California, United States	38.27°N,121.49°W,0m	ESRL	1736(132)	3	1.22	-0.59(-0.46)
'wgc_01p0'	Walnut Grove, California, United States	38.27°N,121.49°W,0m	ESRL	878(0)	1000	0	-4.55(-4.41)
'wis_01d0'	WIS Station, Negev Desert, Israel	31.13°N,34.88°E,400m	ESRL	239(1)	2.5	0.62	-0.1(-0.15)
'wkt_01c3'	Moody, Texas, United States	31.31°N,97.33°W,251m	ESRL	2124(24)	3	0.74	0.11(0.11)
'wkt_01d0'	Moody, Texas, United States	31.31°N,97.33°W,251m	ESRL	168(0)	1000	0	0.15(0.2)
'wkt_01p0'	Moody, Texas, United States	31.31°N,97.33°W,251m	ESRL	979(0)	1000	0	-0.42(-0.45)
'wlg_01d0'	Mt. Waliguan, Peoples Republic of China	36.29°N,100.90°E,3810m	CMA/ESRL	254(19)	1.5	0.83	-0.1(-0.14)
'yon_19c0'	Yonagunijima, Japan	24.47°N,123.02°E,30m	JMA	1684(3)	3	0.78	1.53(1.67)
'zep_01d0'	Ny-Alesund, Svalbard, Norway and Sweden	78.90°N,11.88°E,475m	ESRL	217(2)	1.5	0.75	0.61(0.8)

Table S2 Global annual average aggregated fluxes for TransCom regions from our system compared to similar estimates from CT2011_oi and Peylin et al. (2013). The time span of each of these studies is indicated in the table. All units are Pg C yr^{-1}[a].

	Region Name	prior flux 2006-2010	This work 2006-2010		This work 2008-2010				CarbonTracker 2006-2010	Peylin et al. (2013) 2006-2010	Niwa et al. (2012)
			Case 1	Case 2	Case 3	Case 4	Case 5	Case 6	CT2011_oi[b]	CTE2013[c]	2006-2008
1	North American Boreal	-0.01	-0.23	-0.27	-0.25	-0.26	-0.22	-0.19	-0.21	-0.24	-
2	North American Temperate	-0.12	-0.52	-0.60	-0.63	-0.61	-0.56	-0.56	-0.37	-0.42	-
3	South American Tropical	0.02	0.15	0.12	-0.08	0.00	-0.05	0.00	0.18	0.09	-
4	South American Temperate	-0.07	0.11	0.00	-0.01	0.09	0.07	-0.03	0.08	-0.10	-
5	Northern Africa	0.06	0.06	0.05	0.08	-0.06	0.08	0.10	-0.07	0.00	-
6	Southern Africa	-0.05	0.05	0.06	0.10	-0.04	-0.02	0.05	-0.01	-0.01	-
7	Eurasia Boreal	0.03	-1.02	-0.96	-1.11	-1.25	-0.96	-0.92	-1.00	-0.93	-
8	Eurasia Temperate	-0.11	-0.68	-0.33	-0.70	-0.63	-0.44	-0.36	-0.41	-0.33	-
9	Tropical Asia	0.22	0.15	0.19	0.12	0.08	0.17	0.20	0.14	0.22	-
10	Australia	-0.11	-0.03	-0.02	-0.09	-0.12	-0.11	-0.12	-0.01	-0.06	-
11	Europe	-0.09	-0.48	-0.49	-0.50	-0.45	-0.61	-0.67	-0.51	-0.40	-
12	North Pacific Temperate	-0.50	-0.37	-0.38	-0.37	-0.37	-0.39	-0.40	-0.40	-0.41	-
13	West Pacific Tropical	0.00	0.00	0.00	-0.01	0.00	-0.01	-0.01	0.01	0.00	-
14	East Pacific Tropical	0.22	0.31	0.32	0.34	0.34	0.30	0.31	0.33	0.35	-
15	South Pacific Temperate	-0.53	-0.54	-0.62	-0.58	-0.58	-0.58	-0.52	-0.64	-0.60	-
16	Northern Ocean	-0.25	-0.25	-0.27	-0.26	-0.27	-0.25	-0.25	-0.25	-0.30	-
17	North Atlantic Temperate	-0.50	-0.40	-0.40	-0.38	-0.39	-0.46	-0.46	-0.43	-0.47	-
18	Atlantic Tropical	0.14	0.17	0.17	0.17	0.18	0.16	0.16	0.16	0.18	-
19	South Atlantic Temperate	-0.26	-0.17	-0.15	-0.13	-0.11	-0.18	-0.19	-0.18	-0.15	-
20	Southern Ocean	-0.61	-0.31	-0.28	-0.29	-0.28	-0.33	-0.33	-0.37	-0.29	-
21	Indian Tropical	0.13	0.14	0.14	0.14	0.14	0.14	0.14	0.18	0.15	-
22	Indian Temperate	-0.58	-0.66	-0.68	-0.67	-0.70	-0.67	-0.63	-0.70	-0.68	-
23	Non-optimized	0.00	0.00	0.00	0.00	0.00	0.00	0.00	0.00	0.00	-
24	Global Total	-2.99	-4.50	-4.41	-5.12	-5.30	-4.92	-4.68	-4.49	-4.44	-4.46
25	Global Land	-0.25	-2.43	-2.24	-3.07	-3.25	-2.65	-2.50	-2.20	-2.20	-2.67
26	Global Ocean	-2.74	-2.08	-2.16	-2.04	-2.05	-2.27	-2.18	-2.30	-2.24	-1.79
27	Asia (7,8,9)	0.13	-1.56	-1.09	-1.69	-1.80	-1.23	-1.08	-1.27	-1.05	-
28	NH Land (1,2,7,8,11)	-0.32	-2.93	-2.64	-3.20	-3.20	-2.79	-2.70	-2.50	-2.33	-
29	Tropical Land(3,5,9)	0.30	0.36	0.36	0.13	0.02	0.20	0.30	0.26	0.31	-
30	Southern Land (4,6,10)	-0.22	0.13	0.04	0.00	-0.07	-0.06	-0.10	0.05	-0.18	
31	NH Total (1,2,7,8,11,12,16,17)	-1.56	-3.95	-3.69	-4.21	-4.23	-3.89	-3.81	-3.58	-3.52	-
32	Tropical Total(3,5,9,13,14,18,21)	0.79	0.99	0.99	0.77	0.68	0.79	0.90	0.93	0.99	-
33	Southern Total(4,6,10,15,19,20,22)	-2.21	-1.55	-1.70	-1.67	-1.74	-1.82	-1.77	-1.85	-1.91	

[a]All the terrestrial biosphere fluxes are including land uptake and biomass burning emissions, but excluding fossil fuel emissions.

[b]CT2011_oi : this data is derived from http://carbontracker.noaa.gov

[c]CTE2013 is the result of Carbon Tracker Europe (Peters et al., 2010) as presented in Peylin et al., (2013) for the period of 2006-2010

The estimated (a posterior) global CO_2 sinks/sources across 6 sensitivity tests were presented in Table S2, and aggregated to annual mean for TransCom regions. These experiments form a range around the best estimate, given an alternative uncertainty with upper and lower limits of sensitivity tests to the assimilation system. As previous description, the Case 1 was performed the best assimilation on CO_2 source/sink and its results are used to analyze the global carbon flux. Our inverted results of annual carbon flux in Case 1 (surface−CONTRAIL) shows that most land regions are estimated as carbon sinks, with strong sinks in the Eurasia Boreal, Eurasia Temperate, North American Temperate, North American Boreal and Europe, while Tropical Asia, South America and Africa are inferred as carbon sources. The estimated ocean fluxes show the same tendencies as the *a priori* fluxes that East Pacific Tropical Oceans, Atlantic Tropical Oceans and Indian Tropical Oceans are carbon source, while others are CO_2 sinks. This distribution of carbon sinks/source is reasonable and quite consistent with another inversion estimate (Peylin et al. 2013).

Our best global mean CO_2 flux was estimated to be $-4.50^{-4.41}_{-5.30}$ Pg C yr^{-1} (uncertainty range derived from Cases 1-6) for the period 2006-2010, compared with the global *a priori* flux of −2.99 Pg C yr^{-1}. Note here that the biomass burning emissions (averaged +2.20 Pg C yr^{-1} during the studied period) were included in the inverted flux, but fossil fuel emissions (averaged +8.64 Pg C yr^{-1}) were excluded. For comparison, we included the annual means from Carbon Tracker Europe (Peters et al., 2010, quoted as CTE2013) derived from Peylin et al. (2013) and Carbon Tracker North America (quoted as CT2011_oi, data downloaded from http://carbontracker.noaa.gov) for the same time period and areas. The CT2011_oi estimates the carbon flux of global terrestrial biosphere and oceans were

respectively −2.20 Pg C yr^{-1} and −2.30 Pg C yr^{-1}, while the sink inferred fromCTE2013 was estimated to be −2.20 Pg C yr^{-1} on land and −2.24 Pg C yr^{-1} in the ocean. Our inferred global carbon sinks/source ($-4.50^{-4.41}_{-5.30}$ Pg C yr^{-1}) is well consistent with the CT2011_oi (−4.49 Pg C yr^{-1}) and CTE (−4.44 Pg C yr^{-1}). This consistency can be further represented in the partitioning of the NH land sinks between North America, Asia and Europe. In North America, our result ($-0.75^{-0.75}_{-0.88}$ Pg C yr^{-1}) generally agree with CTE2013 (−0.66 Pg C yr^{-1}) and CT2011_oi (−0.58 Pg C yr^{-1}). In Asia, the inverted result is $-1.56^{-1.07}_{-1.80}$ Pg C yr^{-1}, which is within uncertainty and comparable to CTE2013 (−1.05 Pg C yr^{-1}) and the CT2011_oi (−1.27 Pg C yr^{-1}). In Europe, our result ($-0.48^{-0.45}_{-0.67}$ Pg C yr^{-1}) is in the range of CT2011_oi (−0.51 Pg C yr^{-1}) and CTE2013 (−0.37 Pg C yr^{-1}).

Also, we found that the addition of CONTRAIL data creates a larger carbon sink in Temperate Asia, and in the NH land, at the expense of weak ocean uptake. This shifts the fluxes to a stronger land uptake versus weaker ocean sink, more in line with the results of Niwa et al. (2013) that there existed a stronger terrestrial uptake (−2.67 Pg C yr^{-1}) and a weaker oceans uptake (−1.79 Pg C yr^{-1}) caused by using CONTRAIL data.

Overall, our global, all-land and all-ocean estimates of the CO_2 flux in this period are reasonable.

Table S3 The MODIS land use categories converted to the corresponded Olson, et al. (1985) land types table

	IGBP	Olson, et al. (1985)
0	Water Bodies	18 Non-optimized areas (ice, polar desert,inland seas)
1	Evergreen Needleleaf Forest	1 Conifer Forest
2	Evergreen Broadleaf Forest	5 Tropical Forest
3	Deciduous Needleleaf Forest	1 Conifer Forest
4	Deciduous Broadleaf Forest	2 Broadleaf Forest
5	Mixed Forest	3 Mixed Forest
6	Closed Shrublands	13 Shrub/Tree/Suc
7	Open Shrubland	4 Grass/Shrub
8	Woody Savannas	8 Fields/Woods/Savanna
9	Savannas	13 Shrub/Tree/Suc
10	Grasslands	4 Grass/Shrub
11	Permanent Wetlands	11 Wetland
12	Croplands	14 Crops
13	Urban and Built-up	18 Non-optimized areas (ice, polar desert,inland seas)
14	Cropland/Natural Vegetation Mosaic	14 Crops
15	Snow and Ice	18 Non-optimized areas (ice, polar desert,inland seas)
16	Barren or Sparsely Vegetated	12 Deserts

To assess the impact of land cover map on carbon flux, we used MODIS land cover data (MCD12Q1 version 051 of year 2005) in place of map of Olson et al. (1985). The MODIS land cover map was re-sampled into a 1×1^{o} spatial resolution by selecting the pixels with maximum area, and then was converted into Olson et al. (1985) land types. The conversion strategy from MODIS IGBP categories into Olson et al. (1985) land classification are summarized in Table S3. The processed MODIS data are showed in Fig. S1. We found that this land cover data are very different from that of Olson et al. (1985), which could produce large changes in inverted carbon flux.

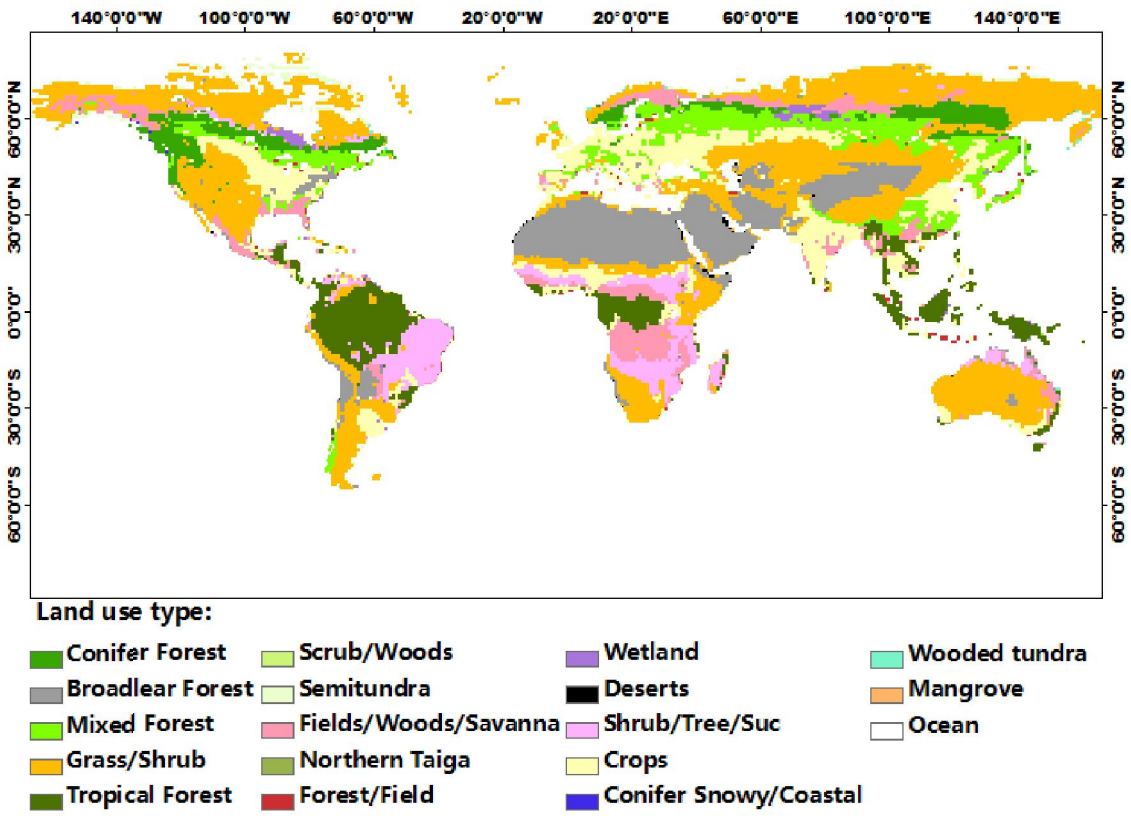

Figure S1 The land use maps (MODIS) used in Case 6